The micro-mechanical behaviour of artificially cemented sand particles under compression and shear

Wanying Wang[1], Vincenzo Nardelli[2] and Matthew R. Coop[3]

ABSTRACT

The mechanical behaviour of cemented sands at the macro-scale has been widely studied in the past, while there is still a lack of laboratory test data for the micro-mechanical response. Therefore, a series of uniaxial compression and tangential shear tests on artificially cemented sand particles have been conducted using a microscope to observe their behaviour. Firstly, the consistency of cemented particles with different cementing agents is discussed. Three breakage modes are proposed according to the images taken using a microscope camera. A new parameter named "local roundness at contact" is introduced to emphasise the effect of contact morphology on the sample strength. Also, the effect of bond thickness on the mechanical response of the cemented particles has been investigated. Finally, the shear strength parameters of artificially cemented sand samples have been determined for two different sample diameters.

[1] City University of Hong Kong

[2] University of Hong Kong, formerly City University of Hong Kong

[3] University College London, formerly City University of Hong Kong

INTRODUCTION

The mechanical characteristics of bonded sands at the macro-scale have been previously studied by conducting laboratory tests, including triaxial and direct shear tests, on both naturally cemented sands and those artificially cemented using, for example, Portland cement or gypsum (e.g. Lade et al., 1989; Airey, 1993; Coop and Atkinson, 1993; Cuccovillo and Coop, 1999; Alvarado et al., 2012). Cook et al. (2011, 2015) emphasised the effect of the microstructure of sandstones including pore size distribution, bond to grain ratio and contact length. According to Jiang et al. (2012a, 2012b), the mode of bond failure was determined by the bond thickness. Thin bonds are formed by a cementing agent filling around the contact between two particles that touch directly, while thick bonds bridge the space between two particles that would not otherwise touch.

Wang and Leung (2008a, 2008b) formulated a DEM model to simulate cementation, emphasising the role of bond breakage and the dilatancy on the cemented sand response. A simpler DEM modelling technique consists of using parallel bonds, but Cheung et al. (2013) found it difficult to obtain an accurate simulation for the behaviour of cemented sandstones because of the large number of parameters required with no existing micro-scale understanding of their likely values, so that they simply had to be calibrated by curve fitting triaxial test data.

While there have been many attempts to model bonds, very few examined their micro-mechanics. This research therefore aimed to explore the behaviour of a pair of artificially cemented particles using a microscope camera to observe the failure modes. Their compression behaviour was investigated along with the shear behaviour. Uniaxial compression tests were performed on particles bonded either with Portland cement or gypsum plaster, but for the shearing behaviour only grains bonded using Portland cement were studied. The compression test configuration is superficially similar to Uniaxial Compression Strength (UCS) tests. However, both the particles and bonds might deform and crush during the compression, each having a different strength and stiffness. Also the geometry of the interface between the two might affect the behaviour. These conditions are therefore more complex than those of UCS tests in which a uniform cylindrical sample is subjected to a nominally uniform stress regime.

APPARATUS AND MATERIALS TESTED

Figure 1 shows the experimental equipment used for the compression tests, which consists of a loading machine and a microscope camera combined with a high intensity lighting system for the camera. During the compression tests, the lower loading platen (1) moved up at 0.1mm/min while the upper frame (2) was fixed, resulting in the cemented particles (3) being compressed uniaxially. Forces and displacements were measured by a load cell (4) with a capacity of 800 N and an LVDT (5) with a precision of about 0.2 μm, mounted below the load cell to eliminate compliance effects. The failure process of the cemented particles was captured by a microscope camera (6) of 50x magnification. Using high intensity lights (7), high quality videos could be made.

The shear tests were carried out using a custom-made Inter-Particle Loading Apparatus (Senetakis et al., 2013) that has been upgraded in order to improve the number of testing modes, its stiffness and accuracy (Nardelli et al., 2016). The apparatus (Fig. 2) consists of a loading frame (a), a sled (b) and three loading arms; each equipped with a micro linear actuator (c) and a load cell (d, capacity: 100 N). The displacements are measured using three non-contact eddy-current sensors (e, resolution: 10^{-5} mm). The two ends of a cemented pair of particles were glued to brass holders using epoxy resin and these were mounted onto the sled and the vertical arm of the apparatus. A shear test was carried out applying a constant vertical force to the sample and then shearing it at a constant displacement rate until breakage occurred. The tangential force was applied along a line that bisected the sample to minimise any bending moments. Two orthogonal digital micro-cameras (f) facilitated the test preparation and monitored the sample response.

Leighton Buzzard sand (LBS) was tested. The particles had dimensions ranging from 2.36 to 5.00 mm and were cleaned by ultrasound, removing oil and dust on the particle surfaces aiming to improve the bonding between the cement and sand. LBS is a quartz sand with few initial internal defects (Zhao et al. 2015). Portland cement (OPC) and gypsum plaster, were used as bonding agents in order to investigate the effect of different bonding materials on the cemented grain strength, making samples of PCLBS and GPLBS, respectively. The water content for each cementing agent was the optimum to achieve the maximum strength, which was around 40% for Portland cement and 25% for gypsum plaster. Two types of custom-made mould were designed for the preparation of samples with a bond diameter of 3 mm and bond thicknesses nominally of 1 or 2 mm. However, the irregularity of the natural shape of the particles, which is quantified later

by their local roundness, led to some variability in the bond thickness, therefore these thicknesses can be considered approximately average values. PCLBS and GPLBS samples were cured for 7 and 2 days, respectively. For each sample new sand particles were used, because they were often damaged during the tests.

It should be highlighted that there are differences between the simplistic geometry of the cemented particles used here and that of real bonded sands. The bonds are wide, having the same diameter as the particles and mostly they were thick. However, cement in natural weak quarzitic sandstones does not tend to be uniformly distributed, but generally tends to cluster at some, but not all, particle contacts, so that the bonds can be thick and wide (e.g. Alvarado et al., 2012), in a not dissimilar fashion to those tested, although sometimes the large bonds would probably contact more than two particles. Making such tiny bonds was challenging and what has been achieved represents only a first, simple step.

For GPLBS, two groups of samples with different contact surface morphologies were prepared (Fig. 3). In one group, the flatter side of the LBS particles contacted with the gypsum bond (a), while in another group, the sharper side contacted the bond (b). The flatter side was identified as the side that the particles came to rest on when dropped onto a surface. The two groups of samples were tested to investigate the influence of contact morphology on the strength.

RESULTS

The investigation of the consistency of mechanical response for each sample in compression was the first step in order to guarantee the reliability of the tests. Both sets of data show considerable scatter and their causes are discussed below. For PCLBS, Figure 4a shows less consistent results and wider variation range in stiffness compared with GPLBS in Figure 4b. Also, the stiffness of GPLBS is higher than that of PCLBS. Figure 4 shows data only for nominal bond thicknesses of 2mm, for which the mean value of peak force of PCLBS is 262 N with a standard deviation of 51 N while that of GPLBS is 364 N with standard deviation of 61 N. A total of 50 samples of GPLBS with 2mm bond thickness were tested, not all of which are shown on Figure 4 for clarity, although this average is for the entire dataset. A further 26 GPLBS samples with bond thickness 1 mm were

tested. The study therefore focussed on the GPLBS because the gypsum plaster performed more consistently as a cementing agent, as is clear in Figure 4.

Breakage modes for GPLBS

Three typical breakage modes for compression were identified for the GPLBS with bond thickness *t* of 2 mm. The images of different loading stages corresponding to the force-displacement curves (Figure 5) for the three modes are illustrated in Figures 6 to 8. Creating a repeatable cement geometry was extremely difficult at this very small size, particularly since the particle sizes and geometries vary. Some small defects can therefore be seen in the cement geometry, however these do not seem to have influenced the failure patterns and their removal would have been impossible without damaging the bonds.

For mode I, the lower particle crushed at point 2 in Figures 5 and 6, corresponding to about 0.8 seconds before the peak point 3, as indicated by the brighter region inside the particle (Figure 6 (2)). Since this bright region is a new and localised feature, it can only result from damage, and Wang and Coop (2016) have shown that it often occurs immediately prior to failure in single particle tests. Failure of some particles could be expected since Wang and Coop had found that this size of single particle typically has peak forces in the range 100-300N, similarly to these tests. It is noted that the particle broke with no immediate effects on the force-displacement response, at least for a small time and displacement interval until at the peak a fracture quickly propagated through the bond vertically, resulting in a sudden drop of the force.

Figure 7 illustrates a typical example for breakage mode II. Once the lower particle broke in Figure 7 (5), as indicated by the bright region, a crack occurred along a single inclined shear band, which involved the whole bond and contact interface. Here the breakage mode is defined by the fracture inclination in the cement, regardless of whether the particle crushed prior to fracture initiation or not. Breakage mode III is a combination of modes I and II. Comparing images in Figures 8 (7) and 8 (8), a small crack, highlighted with a circle, initiated at the upper cement contact interface before the peak in the force-displacement curve. Then it propagated along both the loading axis and an inclined shear band at the same time. In this case, no particle breakage was observed.

Based on the Griffith (1924) criterion, many investigations have been made of the mechanisms of fracture (e.g. Janach, 1977; Batzle et al. 1980; Sammis and Ashby, 1986). For mode I in this study,

the bond failed possibly due to the radial tensile stress within the column, known as "vertical slabbing". The microcracks propagated and combined leading to contiguous vertical failure planes under tension. The growth of a crack inclined to the vertical loading axis as in mode II is more common for compression tests with modest confining pressures. Perhaps the particles contacting the bond might provide some lateral confinement so that the failure occurs in a shear band. In mode III, both the breakage mechanisms apply. It can be concluded that for all modes, while particle breakage may occur first, the bond behaviour dominates the final failure and there is no clear effect of initial particle breakage on the peak strength as all these three examples have similar strengths.

The effect of contact morphology between the particle and bond on the strength

The inconsistency of the peak force of the samples of the same particle size and bond dimension is perhaps related to the different contact morphology between the particles and the bond. To investigate the influence of the contact on the mechanical response, a shape descriptor named Local Roundness (*LR*) has been considered (Wang and Coop, 2016). It describes the sharpness at the contact region of a particle, defined as:

$$LR = \frac{r_c}{R_{ins}}$$

where r_c is the local radius of curvature at the contact region and R_{ins} is the radius of the maximum inscribed circle of the particle outline. A higher *LR* indicates a flatter surface.

Here the average values of *LR* obtained along the contact profile from the two orthogonal images were calculated and the minimum value from the two directions was used, defined as 3D Local Roundness. As mentioned before, two groups of GPLBS samples were prepared obtaining High Local Roundness (*HLR*) samples cementing the flatter sides of the LBS particles (average *LR*=1.92) and Low Local Roundness (*LLR*) samples by using the side opposite the flatter one, (average *LR*=0.43).

Weibull statistics (1951) were used to study the particle strength. Figure 9 shows the effect of local roundness at the interface on the peak force. A high local roundness gives strengths higher than

low local roundness, with characteristic forces of 477 N for *HLR* and 376 N for *LLR*, respectively. Figure 10a illustrates the sand particle breakage ratio for the two groups. For flat contacts (*HLR*), the percentage of LBS breakage is much higher (90%) than that for *LLR* (31%). Therefore, the assemblies with higher strengths are also those where particle breakage occurs (Figure 10b). For the *LLR* particles the lower strength and lack of breakage may result from the stress concentration at the particle/cement interface causing an earlier failure, prior to the particles reaching their strength.

Effect of bond thickness on the sample strength

Figure 11 shows the effect of bond thickness on the strength for the GPLBS. The stresses were calculated as the ratio between the vertical force and the initial horizontal area of the sample, since the radial deformation during the tests could not easily be determined because of their very small size and brittleness. The strengths of cemented particles with 2 mm bonds are slightly higher than those of 1 mm, which probably arises from the complex interaction of the cement and particle failure.

Figure 12a shows the results in terms of stress-strain of 5 compression tests on PCLBS samples having diameter *D*=4 mm and 5 tests for *D*=3 mm. For these earlier tests, the thickness of the bonds was not fixed and it was measured after the end of the tests using a digital calliper assuming that the bond size did not change significantly during the compression stage. The stress-strain curves are characterised by stiffnesses and peak values that are quite variable but not clearly affected by the diameter of the samples. Breakage of the cement bond was observed at the end of every test conducted, with no evidence of particle damage.

The relationship between the maximum normal stress and the sample thickness for all the tests performed on PCLBS is illustrated in Figure 12b. The graph shows a slight increase of peak stress with the cement thickness for both 3 and 4 mm sample diameters, with the possibility of strength bifurcation in for high bond thicknesses (>2mm) which may lead either to higher or lower sample strengths. The strengths measured for both the 3 and 4 mm diameter samples appear to be within the same range but slightly higher peak stresses for those of 3 mm can be observed. This increase of peak strength with the increase of thickness seems in contradiction with the lower strength

values measured from tests on various rock types, where the larger ratios between sample length and diameter correspond to lower sample strengths (Tuncay and Hasancebi, 2009). The results are probably affected by the contact geometry at the interface between the sand grains and the cement bond and by the fact that these samples are not a homogeneous single material like rock samples but complex assemblies of bonded particles. The contrasting effect of thickness for the two bond types also indicates that the bonding material may also play a role.

Shearing behaviour of PCLBS

Figure 13 shows the results of four shear tests on PCLBS samples for 3 and 4 mm diameter samples confined at 1 and 2 N. The force-displacement curves show a clear influence of the confining force on both stiffness and peak values, especially for the 4 mm samples. The failure envelopes for the two groups of samples are illustrated in Figure 14. The scale of the horizontal axis in the graph is enlarged with respect to the vertical for clarity and within the scatter the data are fitted with linear envelopes. The tests were carried out under confining forces between 1 and 3 N, which are far below the strengths measured in uniaxial compression; higher values would lead to tangential forces too high for the apparatus capacity. Very high friction coefficients and a cohesive intercept of sample strength in terms of force were determined, which both increase with the sample diameter (ϕ=53° and 66° and c=2 N and 11 N for 3 and 4 mm diameters, respectively). Therefore, bond diameter has a much clearer effect on tangential strength than on compressive strength. Also, although the scatter of the data lead to uncertain values of c and ϕ, the sample strength clearly increases with the increase of the normal load. This is in agreement with previous research on quartz sands bonded with Portland cement tested using the triaxial apparatus (e.g. Consoli et al., 2012), where an evident increase of strength with confining pressure was observed. In shearing particle breakage was never observed, perhaps because of the low normal loads.

CONCLUSIONS

A series of uniaxial compression and shear tests on cemented particles with different bond thickness, contact morphology and cement agents was performed to investigate the micro-

mechanical behaviour of cemented particles. The data were quite variable, partly as a result of the difficulty of manufacturing such small cemented contacts. In compression, three breakage modes for the GPLBS were proposed: Mode I with cracks that initiate and propagate along the vertical loading axis, while for Mode II they propagate along a single inclined shear band. Mode III is a combination of these two modes. Failure of the bond, rather than that of the particle, is responsible for the peak strength of the assembly.

From research on the continuum behaviour of cemented sands in triaxial tests it has often been assumed that cement breakage would precede particle damage in quartzitic materials because of the strong particles (e.g. Cuccovillo and Coop, 1999). While no particle breakage was seen in shear here, significant particle breakage was seen in compression, although the cement bonds used were relatively large. The contact morphology plays an important role in the sample response and this contributes to the data scatter. Cemented particles with a flatter contact surface between sand and bond tend to be stronger so that there is more damage to the particles. The influence of bond diameter is much less clear in compression than in shearing, for which the strength and stiffness both increased significantly with diameter.

NOTATION

c cohesion intercept

D diameter of the bond

GPLBS   cemented LBS particle using gypsum plaster as cement agent

HLR high local roundness

LLR low local roundness

LR   local roundness

PCLBS   cemented LBS particle using Portland cement as cement agent

r_c local radius of curvature at the contact region

R_{ins} radius of the maximum inscribed circle of the particle outline

t thickness of the bond

ϕ coefficient of friction

REFERENCES

Airey, D. (1993) Triaxial testing of naturally cemented carbonate soil. *Journal of Geotechnical Engineering* 119, No. 9, 1379-1398.

Alvarado, G., Coop, M. R. and Willson, S. (2012) On the role of bond breakage due to unloading in the behaviour of weak sandstones. *Géotechnique* 62, No. 4, 303-316.

Alvarado, G., Liu, N. & Coop, M. R. (2012) The effect of fabric on the behaviour of reservoir sandstones. Canadian Geotech. J. 49 (9), 1036-1051.

Batzle, M. L., Simmons, G and Siegfried, R. W. (1980) Microcrack closure in rock under stress: direct observation. *Journal of geophysical research* 85, No. B12, 7072-7090.

Cheung, L. Y. G, O'Sullivan, C. and Coop, M. R. (2013) Discrete element method simulations of analogue reservoir sandstones. *International journal of Rock Mechanics and Mining Science* 63, 93-103.

Consoli, N.C., Cruz, R.C., Viana Da Fonseca, A. and Coop, M.R. (2012) Influence of cement-voids ratio on stress-dilatancy behavior of artificially cemented sand. *Journal of Geotechnical and Geoenvironmental Engineering* 138, No. 1, 100-109.

Cook, J. E., Goodwin, L. B. and Boutt, D. F. (2011) Systematic diagenetic changes in the grain-scale morphology and permeability of a quartz-cemented quartz arenite. *AAPG Bulletin* 95, No. 6, 1067-1088.

Cook, J. E., Goodwin, L. B., Boutt, D. F. and Tobin, H. J. (2015) The effect of systematic diagenetic changes on the mechanical behavior of a quartz-cemented sandstone. *Geophysics* 80, No. 2, 145-160.

Coop, M. R. and Atkinson, J. H. (1993) The mechanics of cemented carbonate sands. *Géotechnique* 43, No. 1, 53-67.

Cuccovillo, T. and Coop, M. R. (1999) On the mechanics of structured sands. *Géotechnique* 49, No. 6, 741-760.

Griffith, A.A., (1924) The theory of rupture. *Proceedings of the first International Congress for Applied Mechanics*, *Delft*, 55–63.

Janach, W. (1977) Failure of granite under compression. *International Journal of Rock Mechanics and Mining Sciences & Geomechanics Abstracts* 14, No. 4, 209-215.

Jiang, M. J., Sun, Y.G., Li, L.Q., and Zhu, H.H. (2012a) Contact behavior of idealized granules bonded in two different interparticle distances: An experimental investigation. *Mechanics of Materials* 55, 1-15.

Jiang, M. J., Sun, Y. G. and Xiao, Y. (2012b) An experimental investigation on the mechanical behavior between cemented granules. *Geotechnical Testing Journal* 35, No. 5, 678-690.

Lade, P. V. and Overton, D. D. (1989) Cementation effects in frictional materials. *Journal of Geotechnical Engineering* 115, No. 10, 1373-1387.

Nardelli, V., Coop, M. R., Vitone, C. and Chen, S. (2016) The inter-scale behaviour of two natural scaly clays. *Géotechnique Letters* 6, 205-210.

Sammis, C. G. and Ashby, M. F. (1986) The failure of brittle porous solids under compressive stress states. *Acta Metallurgica* 34, No. 3, 511-526.

Senetakis, K., Coop, M. R. and Todisco, M. C. (2013) Tangential load–deflection behaviour at the contacts of soil particles. *Géotechnique Letters* 3, 59-66.

Tuncay, E. and Hasancebi, N. (2009) The effect of length to diameter ratio of test specimens on the uniaxial compressive strength of rock. *Bulletin of Engineering Geology and Environment* 68, 491-497.

Wang, Y. H. and Leung, S. C. (2008a) A particulate-scale investigation of cemented sand behaviour. *Canadian Geotechnical Journal* 45, No. 1, 29-44.

Wang, Y. H. and Leung, S. C. (2008b) Characterization of cemented sand by experimental and numerical investigations. *Journal of Geotechnical and Geoenvironmental Engineering* 134, No. 7, 992-1004.

Wang, W. and Coop, M.R. (2016) An investigation of breakage behaviour of ingle sand particles using a high-speed microscope camera. *Géotechnique* 66, No. 12, 984-998.

247.

Weibull, W. (1951) A statistical distribution function of wide applicability. *Journal of Applied Mechanics* 18, 293-297.

Zhao, B., Wang, J., Coop, M. R., Viggiani G. and M. Jiang (2015) An investigation of single sand particle fracture using X-ray micro-tomography. *Géotechnique* 65, No. 8, 625-641.
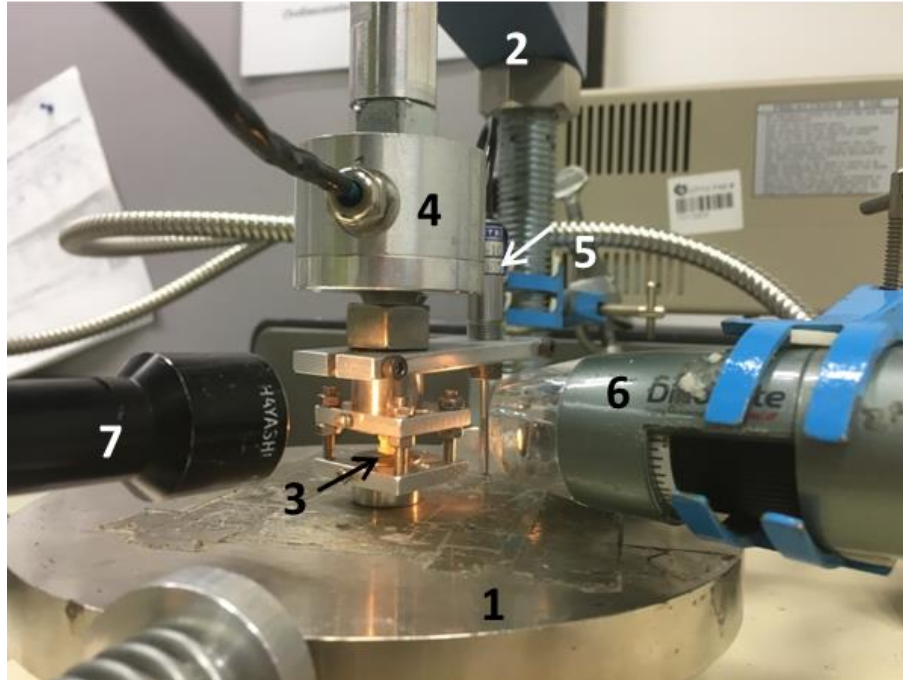
Fig. 1. Testing apparatus for uniaxial compression tests 1) lower loading platen 2) upper frame 3) cemented particles 4) load cell 5) LVDT 6) digital microscope camera 7) high intensity fibre-optic lights.
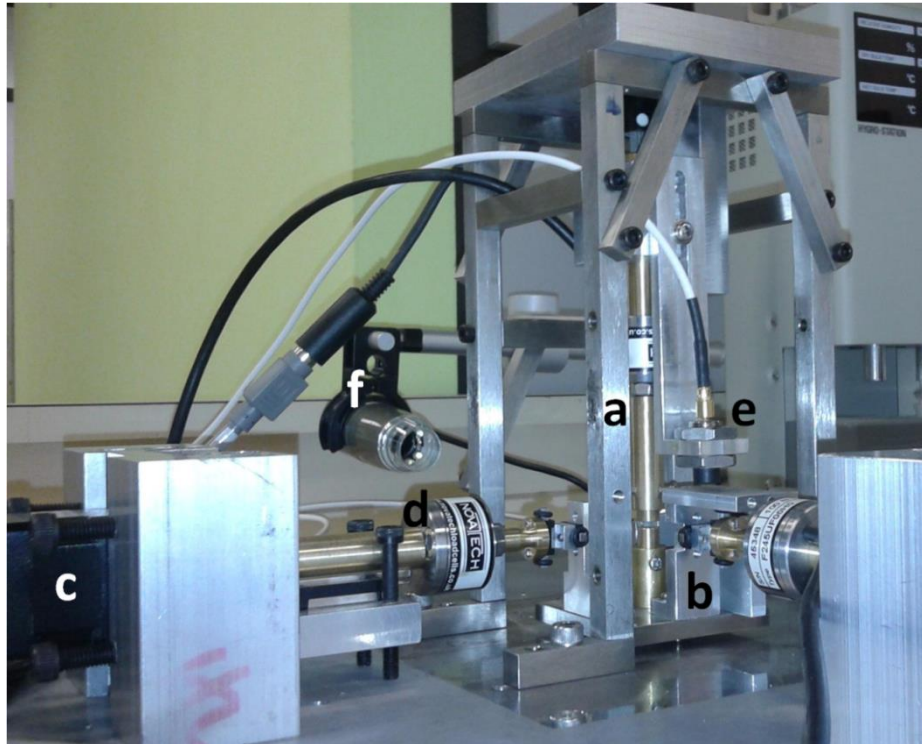
Fig. 2. Inter-particle loading apparatus for shear tests: a) loading frame; b) sled; c) micro-linear actuator; d) high resolution load cell; e) eddy-current displacement sensor; f) digital microscope.
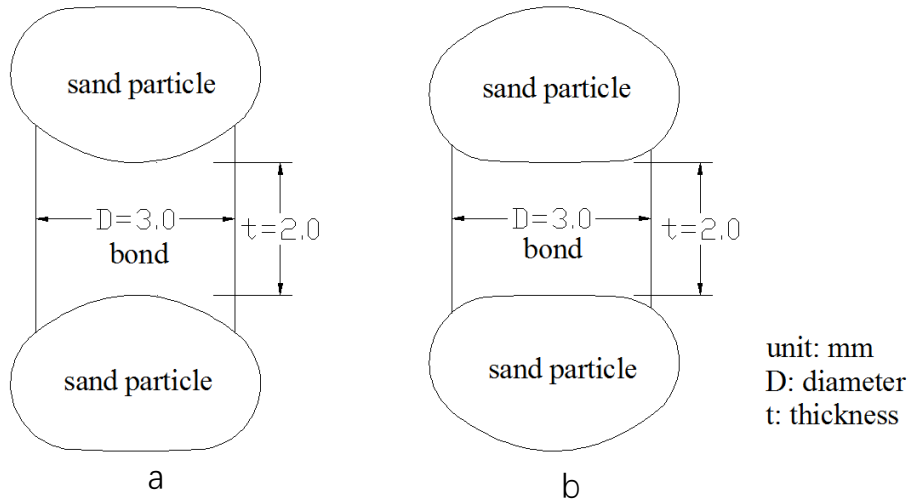
Fig. 3. Different cemented particle configurations a) low local roundness at contact b) high local roundness at contact.
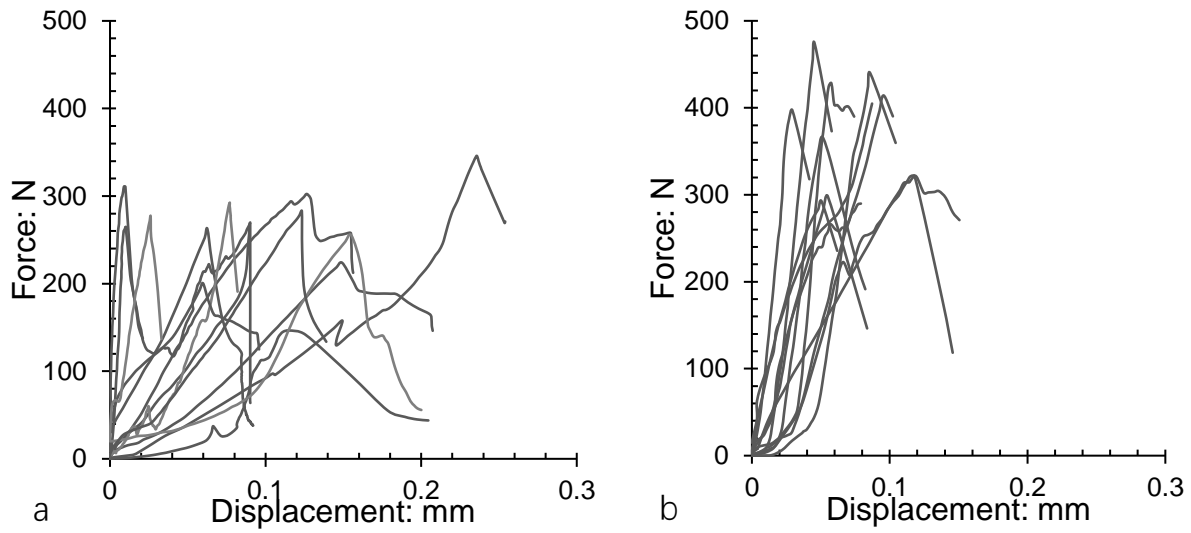
Fig. 4. Consistency of cemented LBS particles with bond thickness of 2 mm tested in compression a) Portland cement b) gypsum plaster.
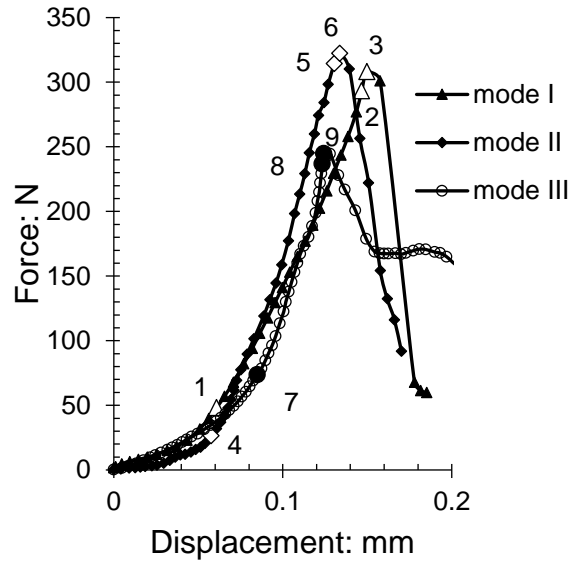
Fig. 5. Force-displacement curves for gypsum cemented particles for breakage modes I, II and III.
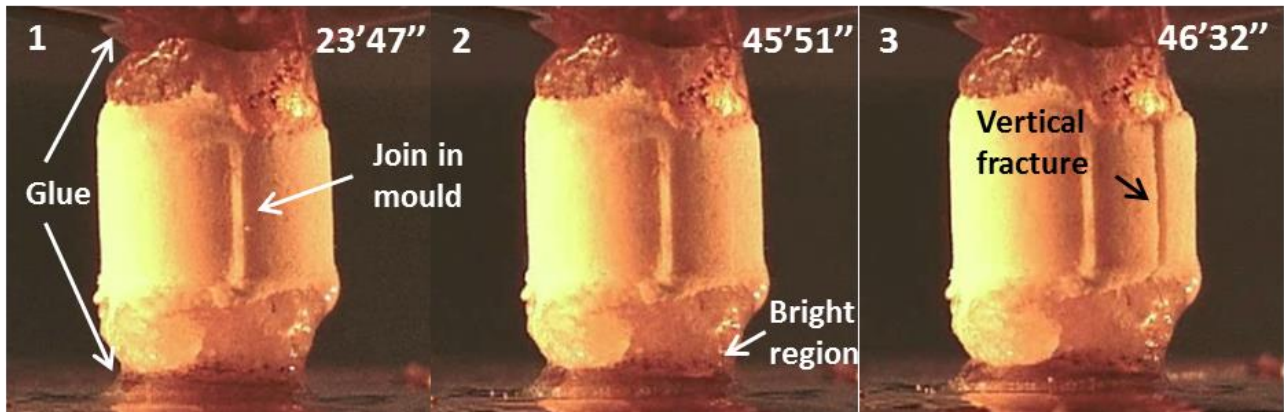
Fig. 6. Breakage mode I: crack in the bond occurs along the loading direction.
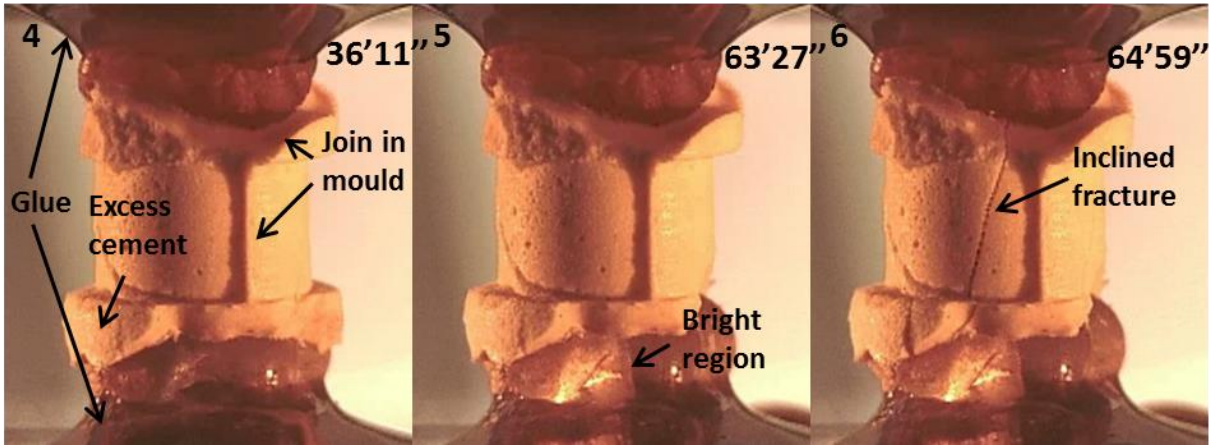
Fig. 7. Breakage mode II: crack in the bond occurs along a single inclined shear band which involved the whole bond.
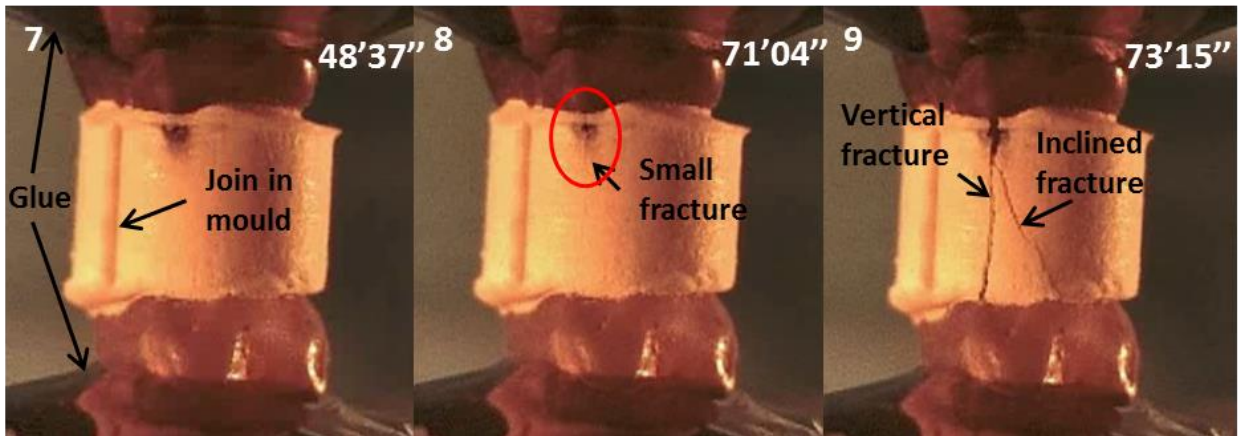
Fig. 8. Breakage mode III: crack in the bond occurs along loading direction and inclined shear band which involved the whole bond.
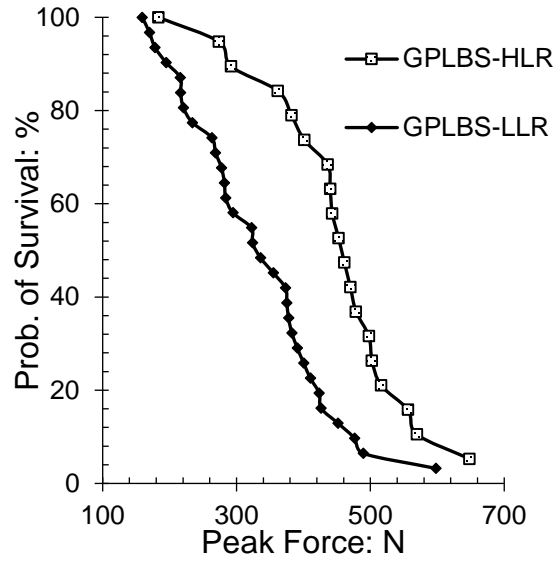
Fig. 9. The effect of particle local roundness at contact surface on the peak force of the cemented particles.
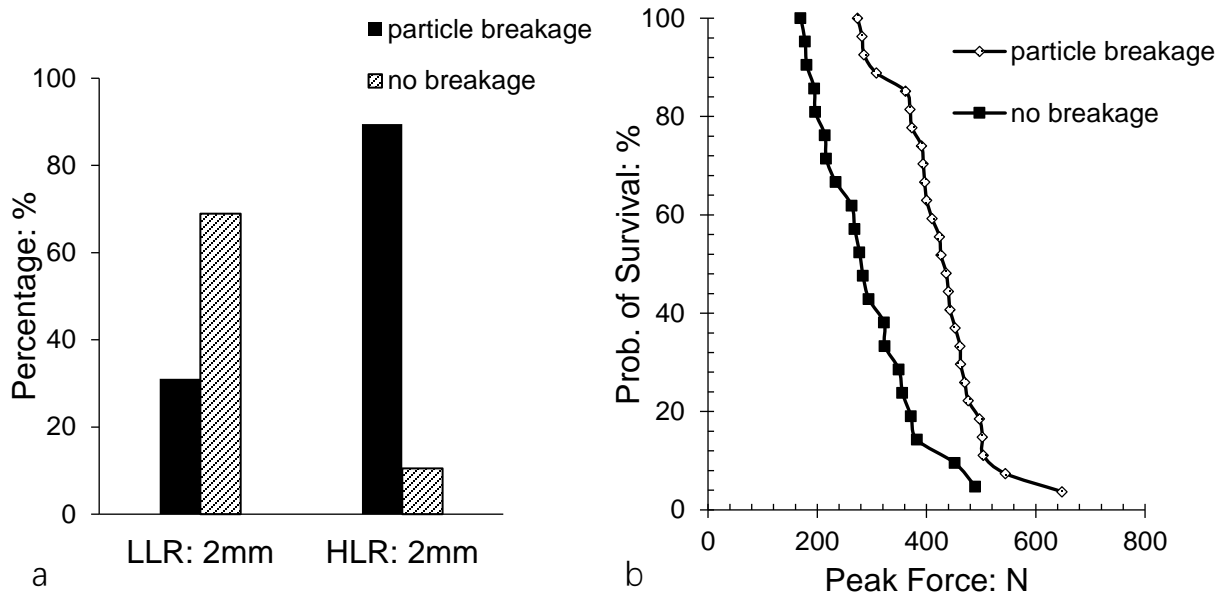
Fig. 10 a) The LBS particle breakage ratio for cemented particles with different particle local roundness at the contact surface, b) The effect of the peak force on particle breakage.
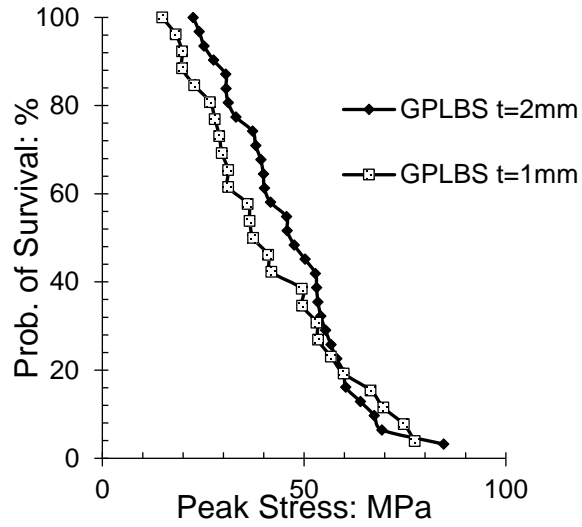
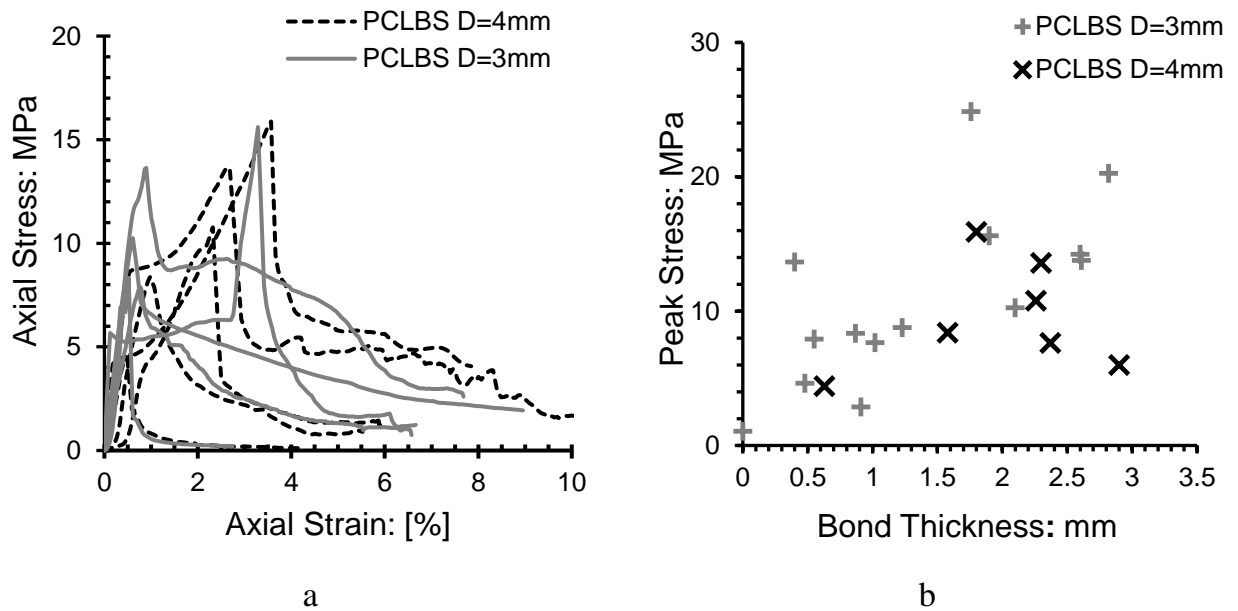Fig. 11. The effect of bond thickness on the strength distribution of GPLBS particles.

a

b

Fig. 12. a) Compression test results for PCLBS samples; b) effect of bond thickness on the peak strength of PCLBS.
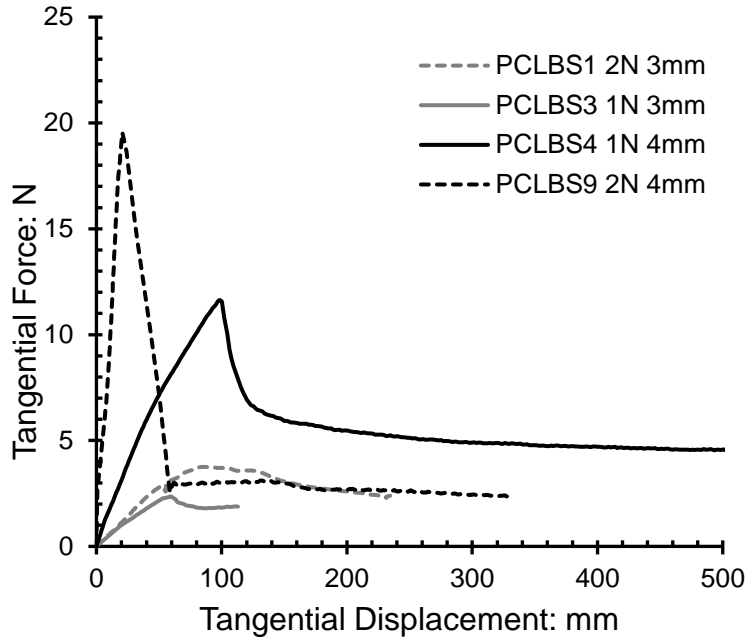
Fig. 13. Shear test results on PCLBS samples having different diameters (3 and 4 mm).
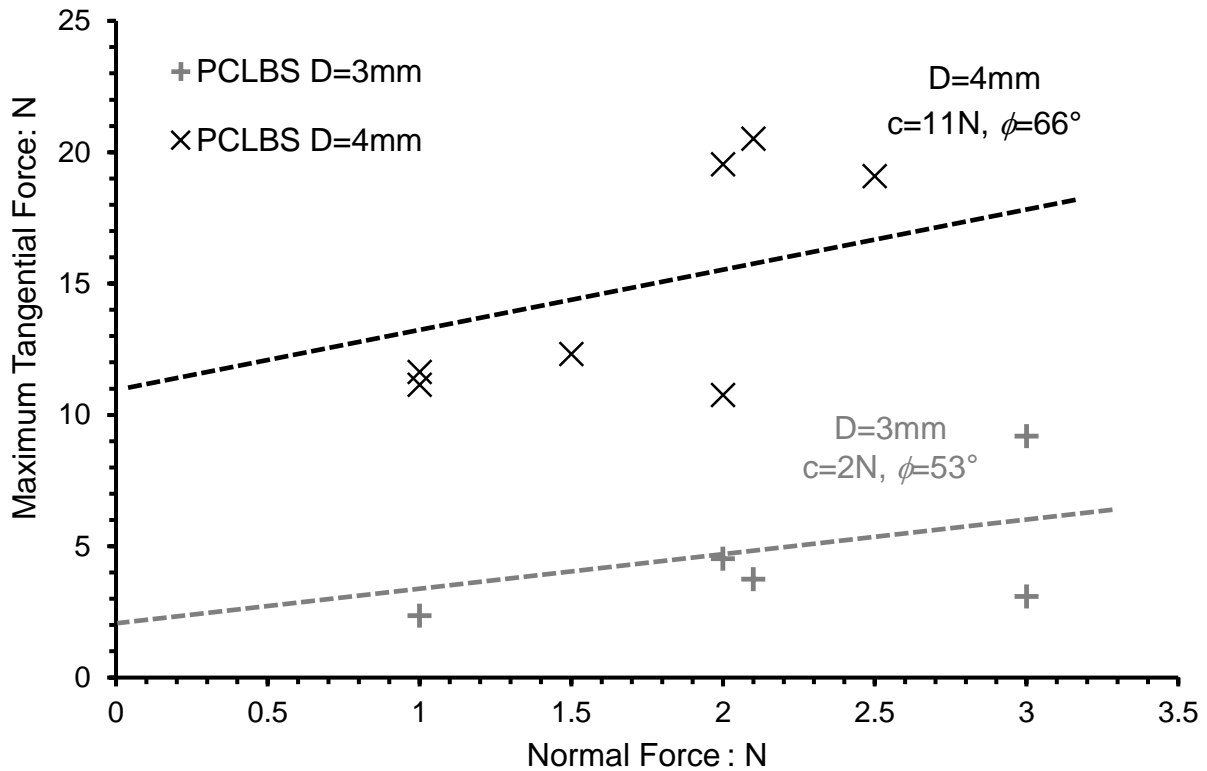

Fig. 14. Possible failure envelopes for PCLBS samples having different diameters (3 and 4mm) tested in shearing.